

Electronic Supplementary Material (ESI)

**Remarkable synergy of borate and interfacial hole transporter on  
BiVO<sub>4</sub> photoanodes for photoelectrochemical water oxidation**

Qijun Meng <sup>a</sup>, Biaobiao Zhang <sup>b,c\*</sup>, Hao Yang <sup>a</sup>, Chang Liu <sup>d</sup>, Yingzheng Li <sup>d</sup>, Oleksandr Kravchenko <sup>a</sup>, Xia Sheng <sup>a</sup>, Lizhou Fan <sup>a</sup>, Fusheng Li <sup>d</sup>, Licheng Sun <sup>a,b,c,d\*</sup>

<sup>a</sup> Department of Chemistry, KTH Royal Institute of Technology, 10044 Stockholm, Sweden

<sup>b</sup> Center of Artificial Photosynthesis for Solar Fuels, School of Science, Westlake University, 310024 Hangzhou,  
China

<sup>c</sup> Institute of Natural Sciences, Westlake Institute for Advanced Study, Hangzhou, 310024 Zhejiang,  
China

<sup>d</sup> State Key Laboratory of Fine Chemicals, Institute of Artificial Photosynthesis, DUT-KTH Joint Education and Research Center on Molecular Devices, Dalian University of Technology (DUT), 116024 Dalian, China

\*Corresponding author Email:

[zhangbiaobiao@westlake.edu.cn](mailto:zhangbiaobiao@westlake.edu.cn)

[lichengs@kth.se](mailto:lichengs@kth.se)

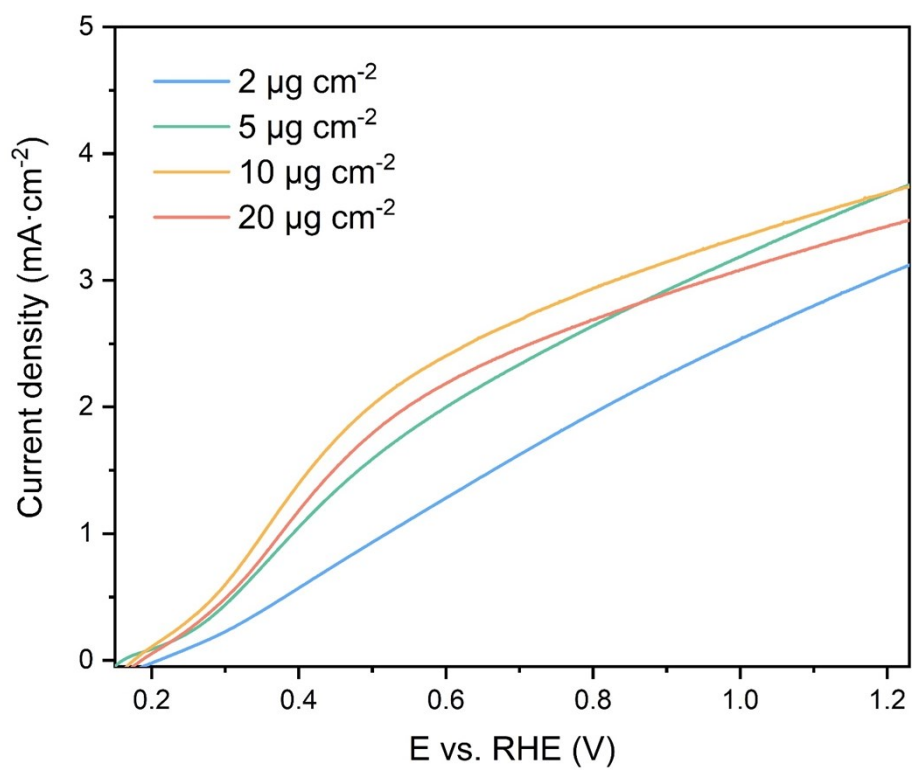


**Fig. S1.** LSV curves for NiFeV/BiVO<sub>4</sub> photoanodes with a series of catalyst mass loading measured under AM 1.5G illumination in a 1.0 M potassium borate buffer at pH 9.3 (scan rate: 10 mV s<sup>-1</sup>).

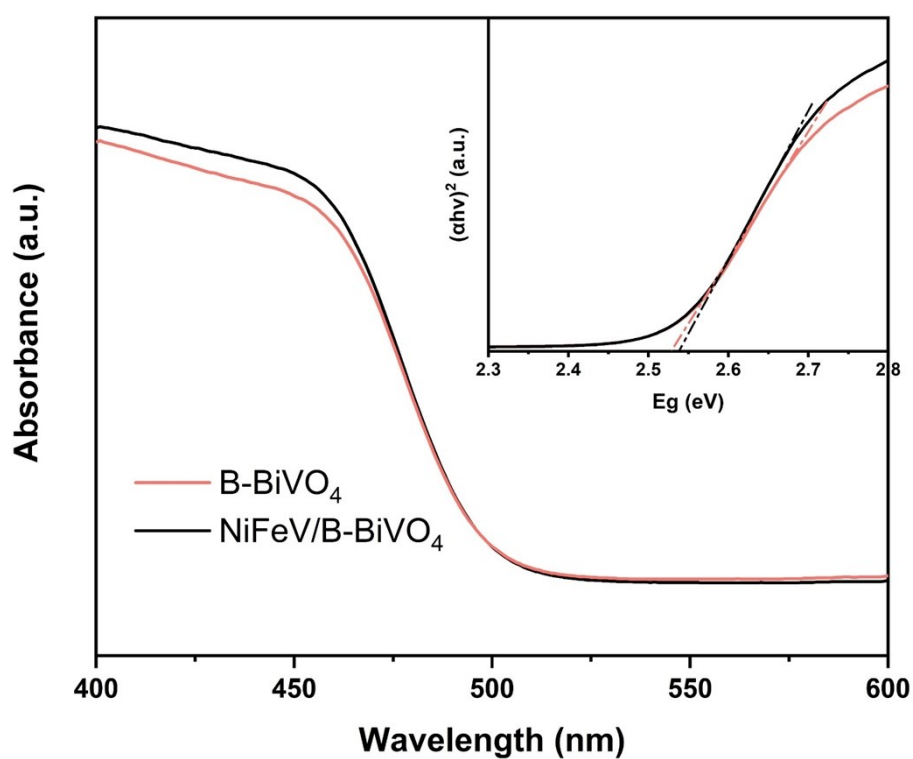


**Fig. S2.** UV-Vis diffuse spectra of B-BiVO<sub>4</sub> and NiFeV/B-BiVO<sub>4</sub> photoanodes, and the inset are corresponding Tauc plots

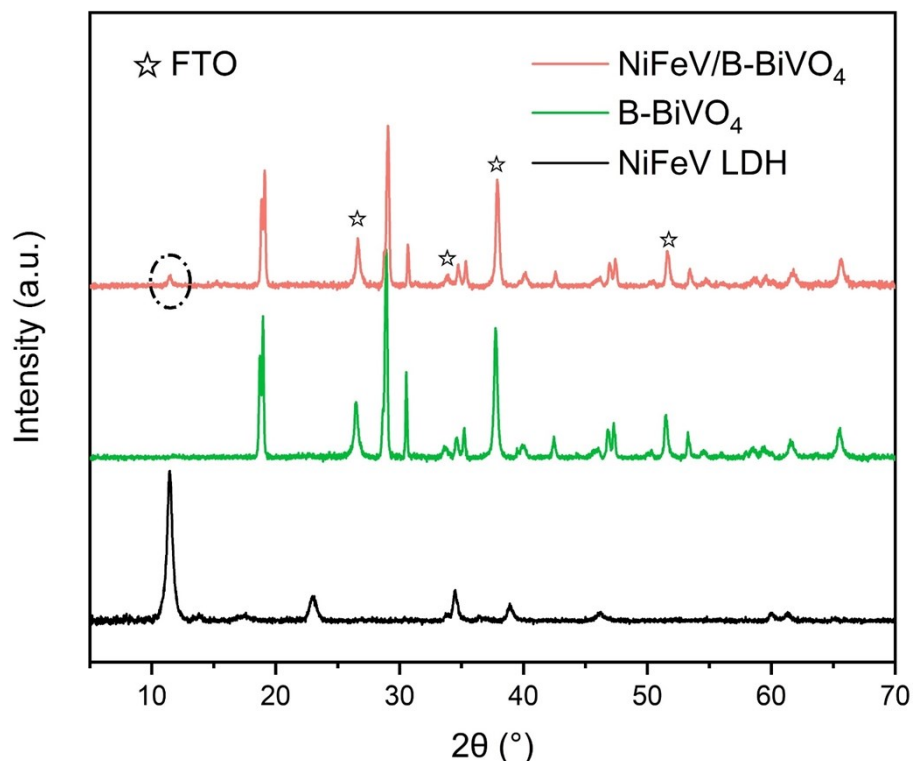


**Fig. S3.** XRD spectra of NiFeV LDH, BiVO<sub>4</sub>, B-BiVO<sub>4</sub> and NiFeV/B-BiVO<sub>4</sub> photoanodes.

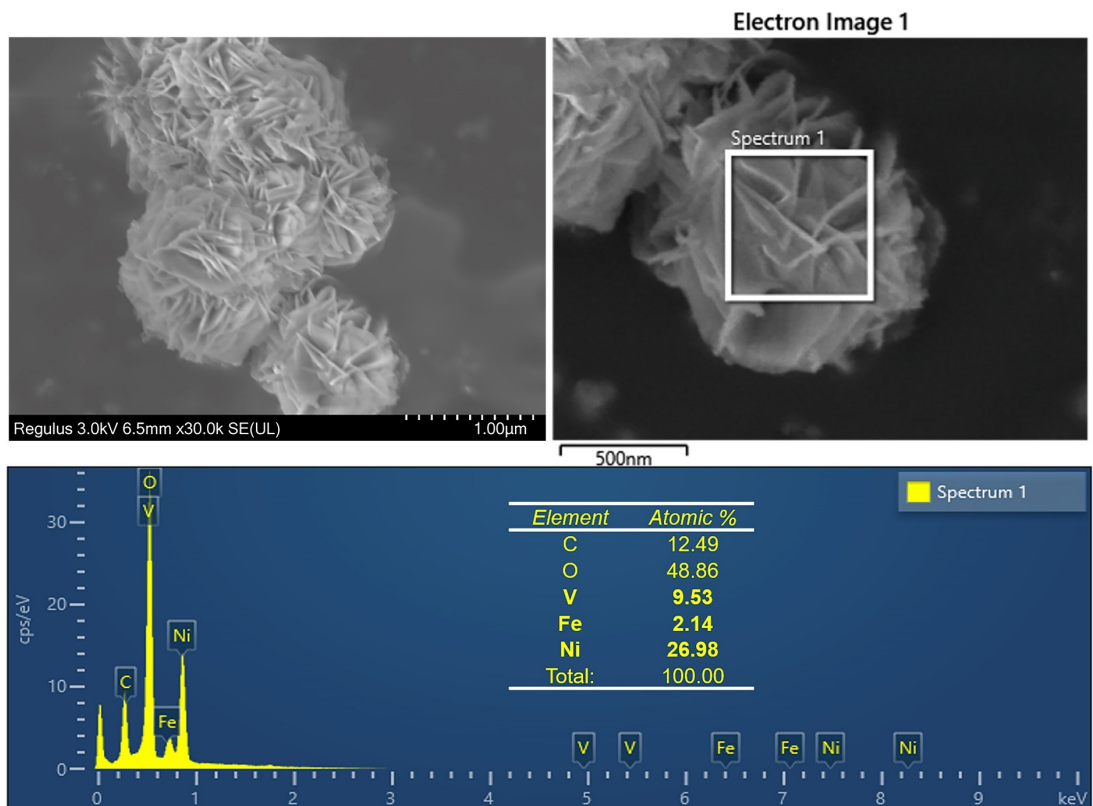


**Fig. S4.** FE-SEM images (upper) and EDX patterns (bottom) with corresponding element ratio of NiFeV LDHs.

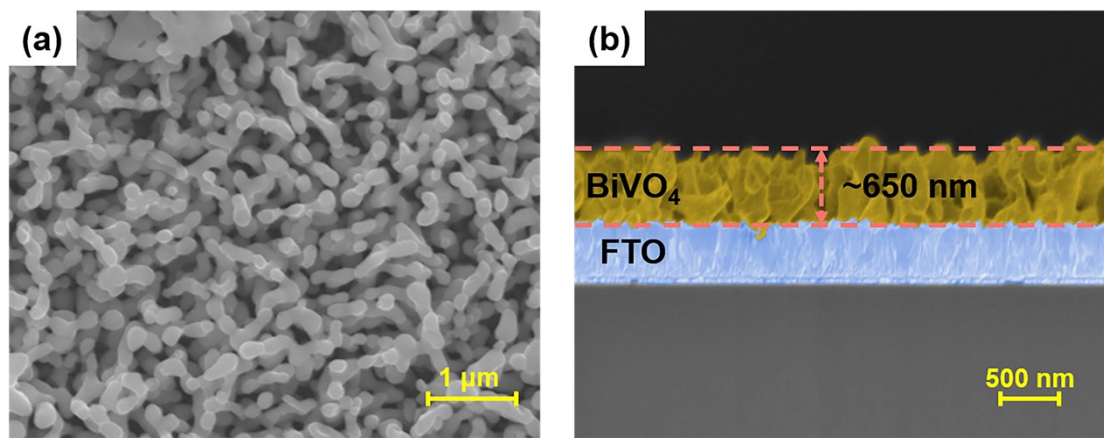


**Fig. S5.** **(a)** The top-view and **(b)** cross-sectional SEM images of the bare BiVO<sub>4</sub> photoelectrode.

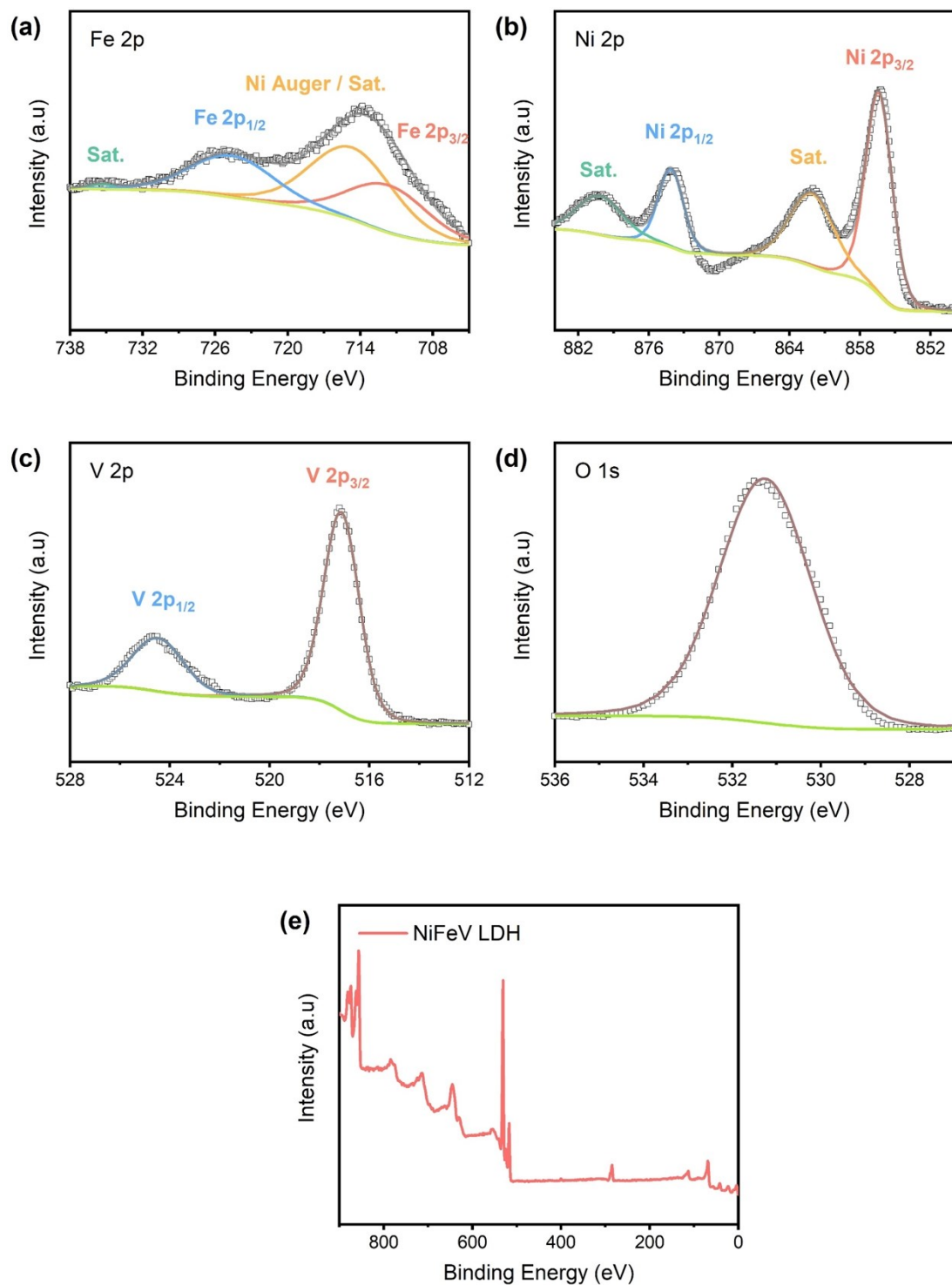


**Fig. S6.** XPS high-resolution spectra of pure NiFeV LDHs: (a) Ni 2p, (b) Fe 2p, (c) V 2p, (d) O 1s, and (e) the corresponding XPS survey.

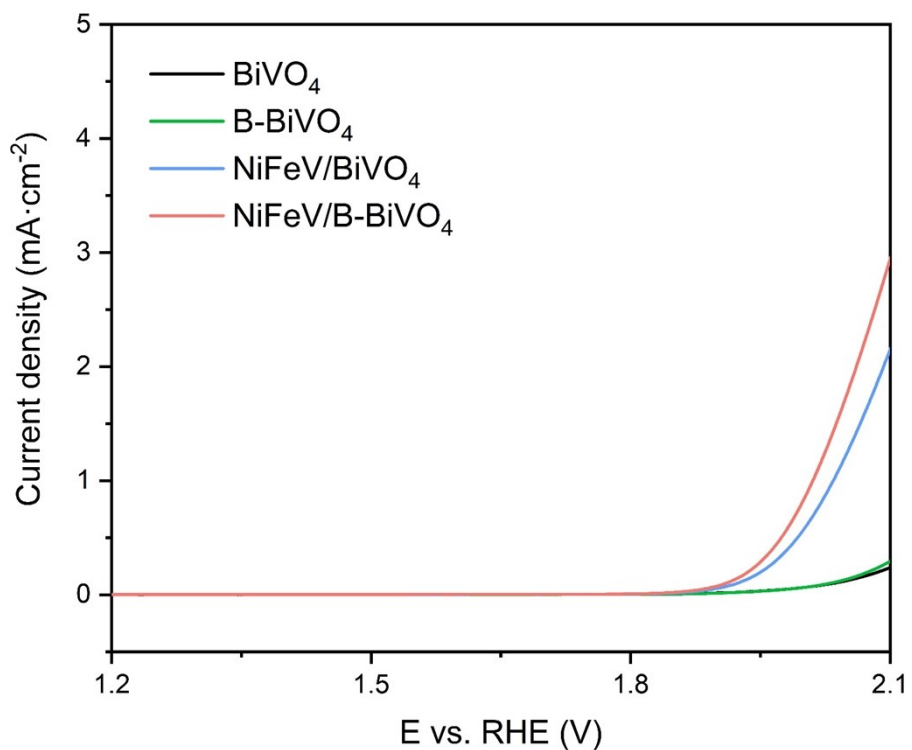


**Fig. S7.** LSV curves of BiVO<sub>4</sub>, B-BiVO<sub>4</sub>, NiFeV/BiVO<sub>4</sub>, and NiFeV/B-BiVO<sub>4</sub> photoanodes in dark in a 1.0 M potassium borate buffer at pH 9.3 (scan rate: 10 mV s<sup>-1</sup>).

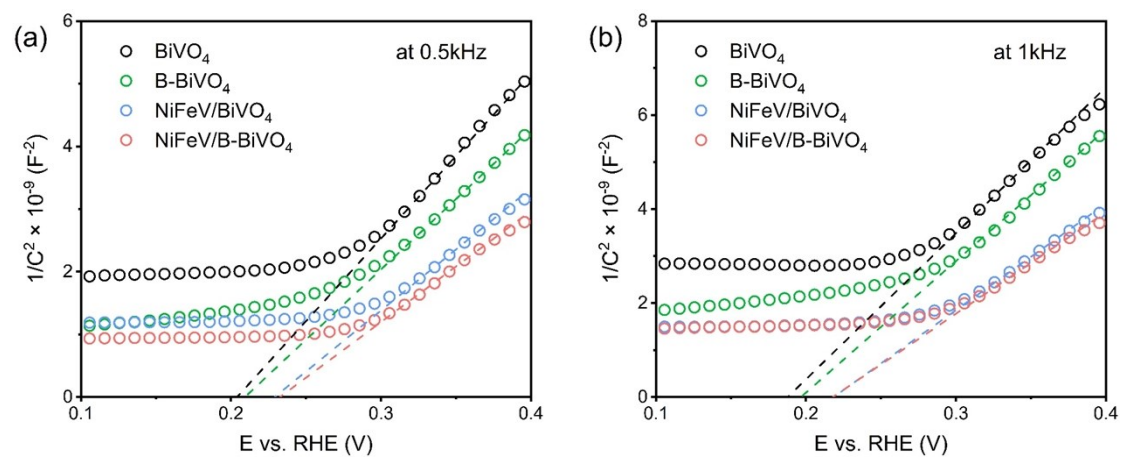


**Fig. S8** Mott-Schottky (MS) plots of photoanodes in dark at **(a)** 0.5 kHz and **(b)** 1 kHz.

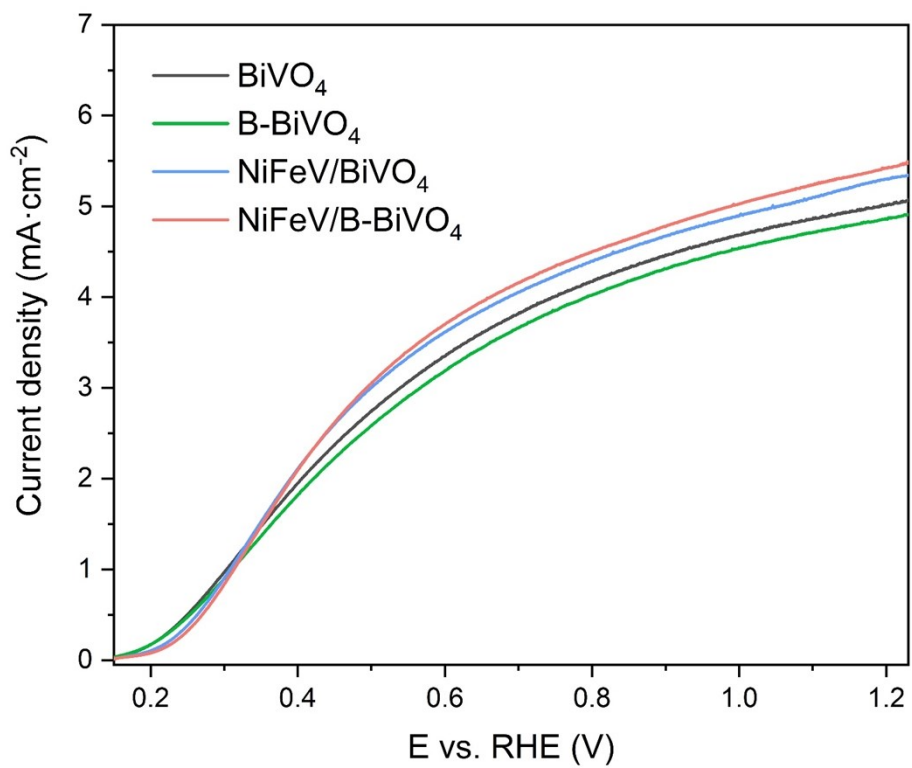


**Fig. S9.** LSV curves of  $\text{BiVO}_4$ ,  $\text{B-BiVO}_4$ ,  $\text{NiFeV/BiVO}_4$ , and  $\text{NiFeV/B-BiVO}_4$  photoanodes under AM 1.5G illumination in a 1.0 M potassium borate buffer (pH 9.3) with 0.2 M  $\text{Na}_2\text{SO}_3$  (scan rate: 10 mV s<sup>-1</sup>).

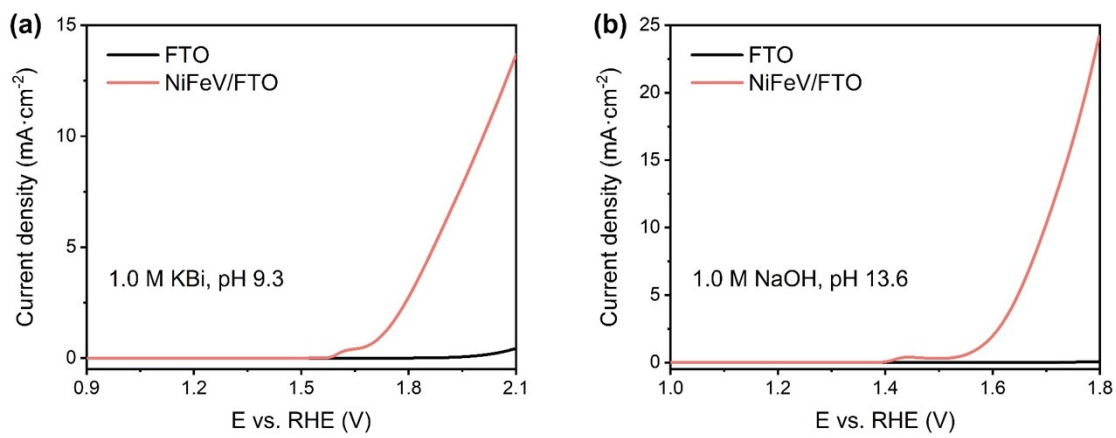


**Fig. S10.** The LSV measurements of NiFeV/FTO in **(a)** 1.0 M potassium borate buffer (pH 9.3) and **(b)** 1.0 M NaOH solution (pH 13.6) at a scan rate of  $50 \text{ mV s}^{-1}$  with 95% iR compensation.

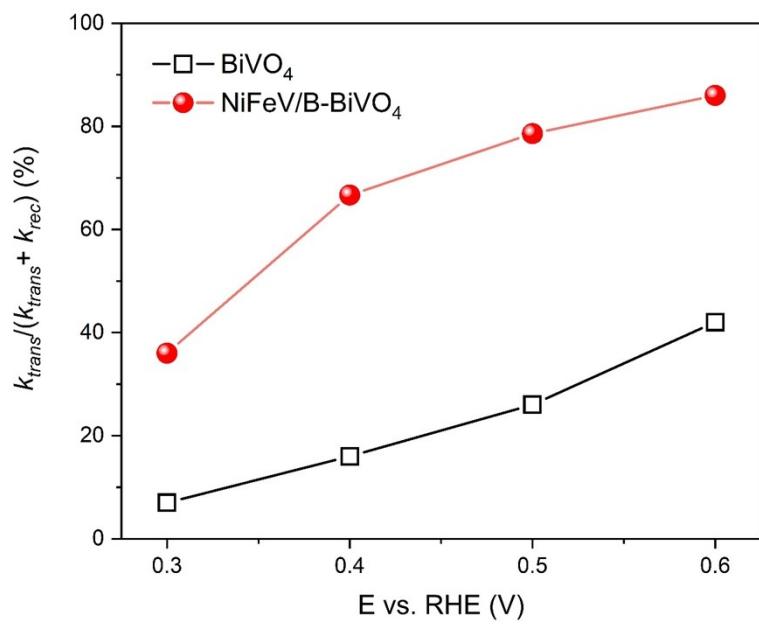


**Fig. S11.** The surface charge transfer efficiency, in terms of  $k_{trans}/(k_{trans}+k_{rec})$  for the BiVO<sub>4</sub> and NiFeV/B-BiVO<sub>4</sub> photoanodes obtained from IMPS analysis.

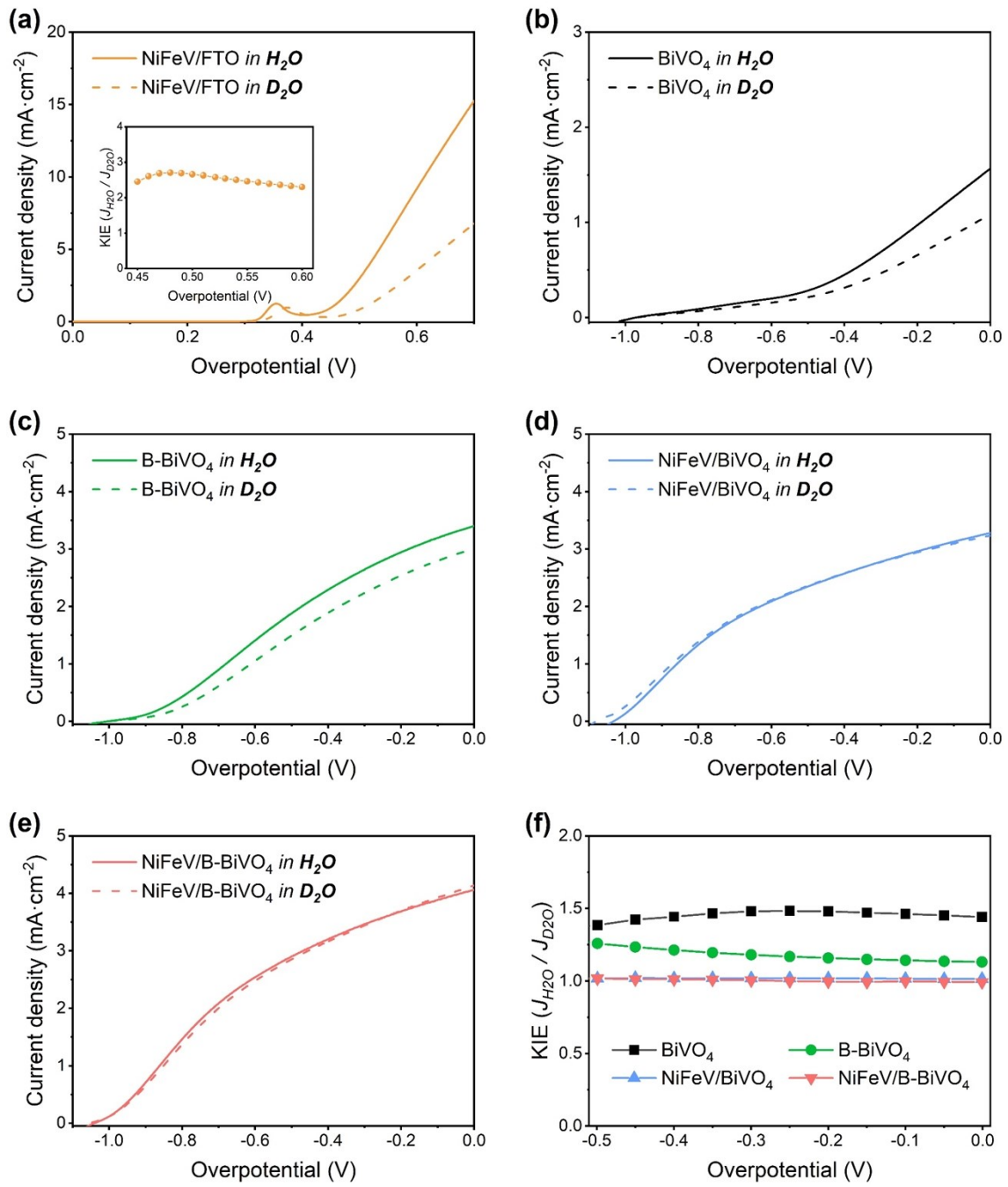


**Fig. S12.** **(a)** LSV curves of NiFeV/FTO in 0.1 M sodium borate  $\text{H}_2\text{O}$  (solid line) and  $\text{D}_2\text{O}$  (dash line) solutions, respectively (scan rate of 10 mV s<sup>-1</sup> and 95% iR compensation); and the inset exhibits the corresponding KIEs at different overpotentials. **(b)** BiVO<sub>4</sub>, **(c)** B-BiVO<sub>4</sub>, **(d)** NiFeV/BiVO<sub>4</sub> and **(e)** NiFeV/B-BiVO<sub>4</sub> photoanodes tested under light illumination in 0.1 M sodium borate  $\text{H}_2\text{O}$  (solid line) and  $\text{D}_2\text{O}$  (dash line) solutions, respectively. **(f)** Corresponding KIE values of photoanodes *versus* overpotential.

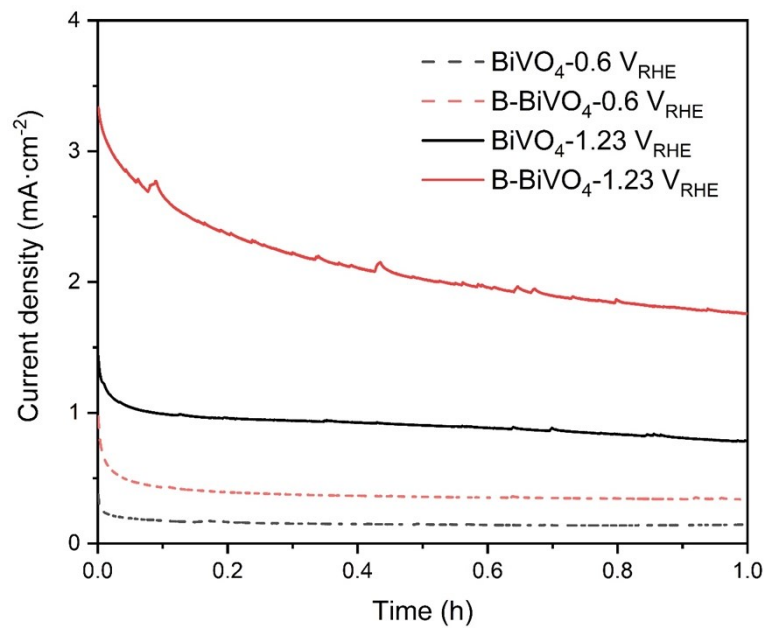


**Fig. S13.**  $J$ - $t$  curves of BiVO<sub>4</sub> and B-BiVO<sub>4</sub> tested in a 1.0 M potassium borate buffer (pH 9.3) at 0.6 V<sub>RHE</sub> and 1.23 V<sub>RHE</sub>, respectively.

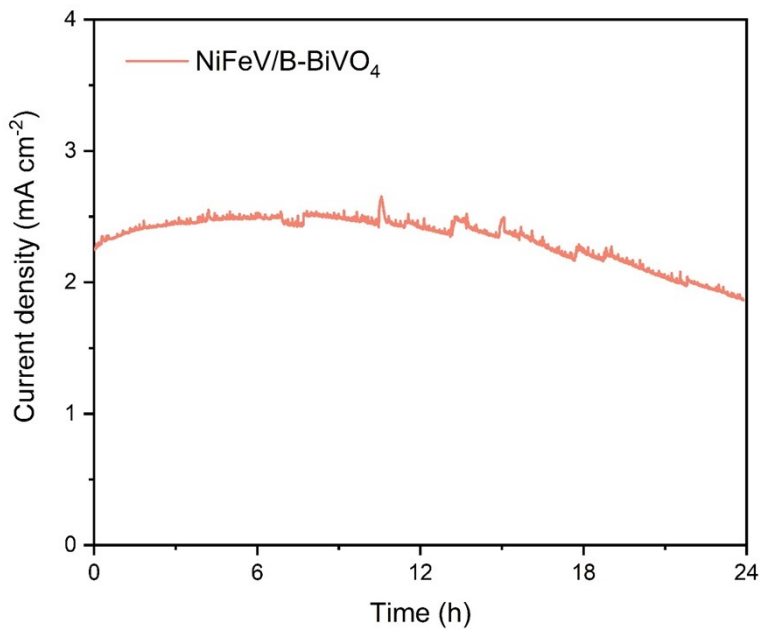


**Fig. S14.** The  $J$ - $t$  curve of NiFeV/B-BiVO<sub>4</sub> tested in a 1.0 M potassium borate buffer (pH 9.3) at 0.6 V<sub>RHE</sub> for 24 h.

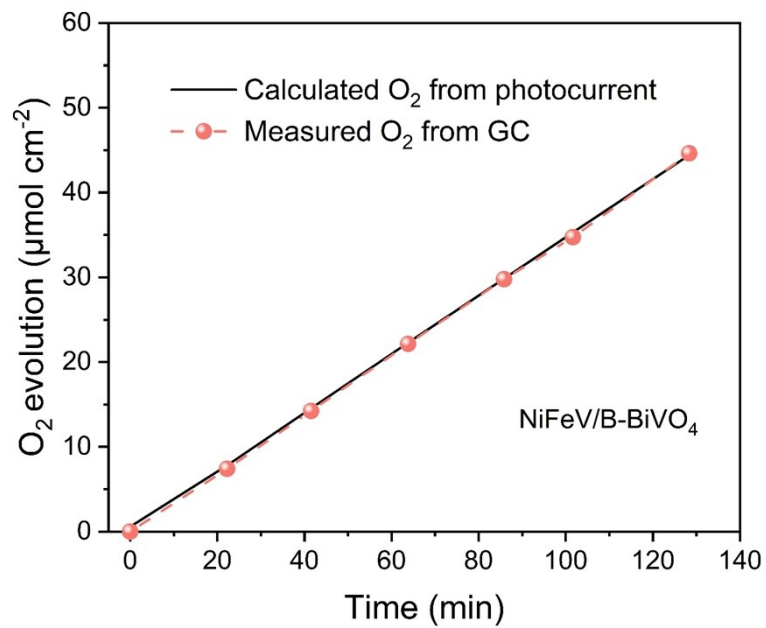
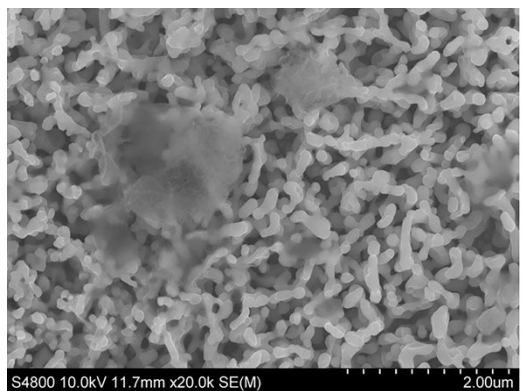
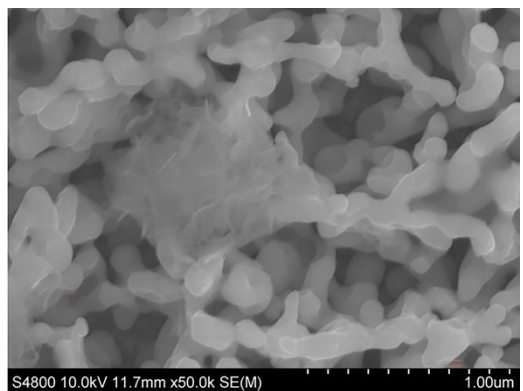


**Fig. S15.** Oxygen evolutions detected by gas chromatography and calculated from photocurrent during the photolysis of NiFeV/B-BiVO<sub>4</sub> photoanode at 0.6 V<sub>RHE</sub>.



S4800 10.0kV 11.7mm x20.0k SE(M)



S4800 10.0kV 11.7mm x50.0k SE(M)

**Fig. S16.** The top-view SEM images of NiFeV/B-BiVO<sub>4</sub> at different magnifications after *J-t* testing at 0.6 V<sub>RHE</sub> for 8 h.

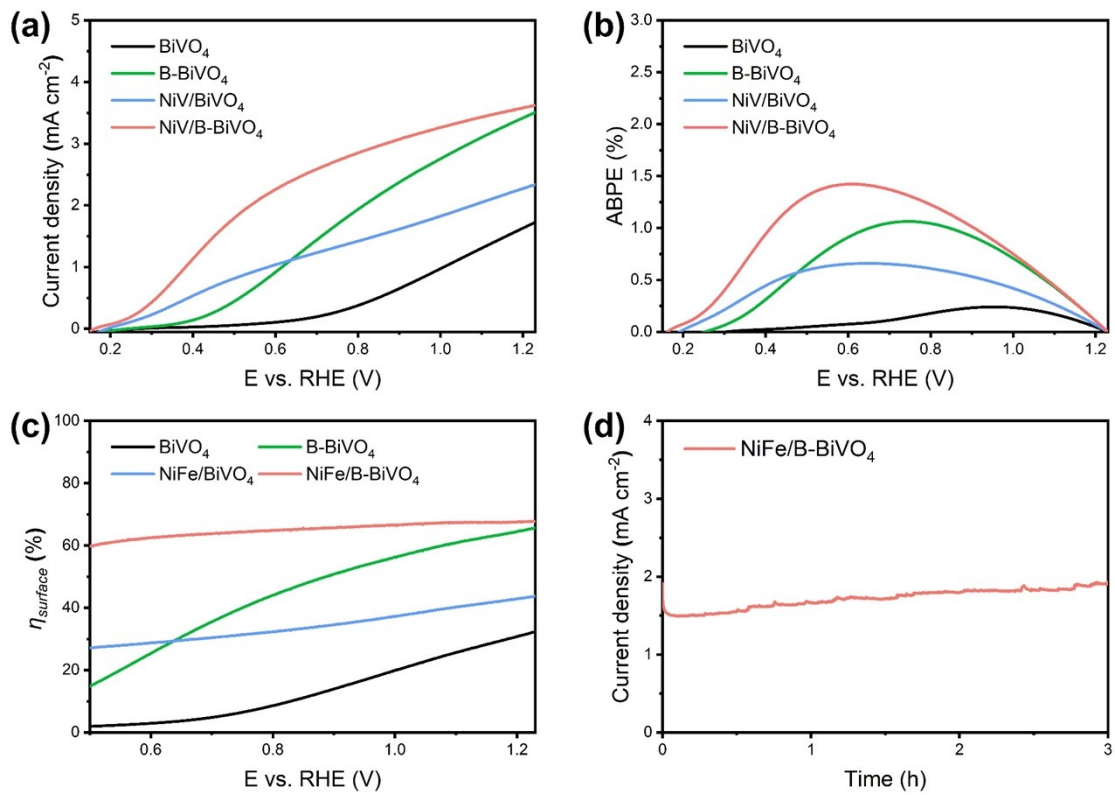


**Fig. S17.** **(a)** LSV curves of  $\text{BiVO}_4$ ,  $\text{B-BiVO}_4$ ,  $\text{NiFe/BiVO}_4$ , and  $\text{NiFe/B-BiVO}_4$  photoanodes under AM 1.5G illumination in a 1.0 M potassium borate buffer at pH 9.3 (scan rate:  $10 \text{ mV s}^{-1}$ ); **(b)** ABPE curves of photoanodes calculated from LSV curves; **(c)** Surface charge transfer efficiency ( $\eta_{\text{surface}}$ ) of photoanodes obtained from LSV curves of water oxidation and sulfite oxidation; **(d)** Long-term  $J-t$  curves at a constant bias of  $0.6 \text{ V}_{\text{RHE}}$ .

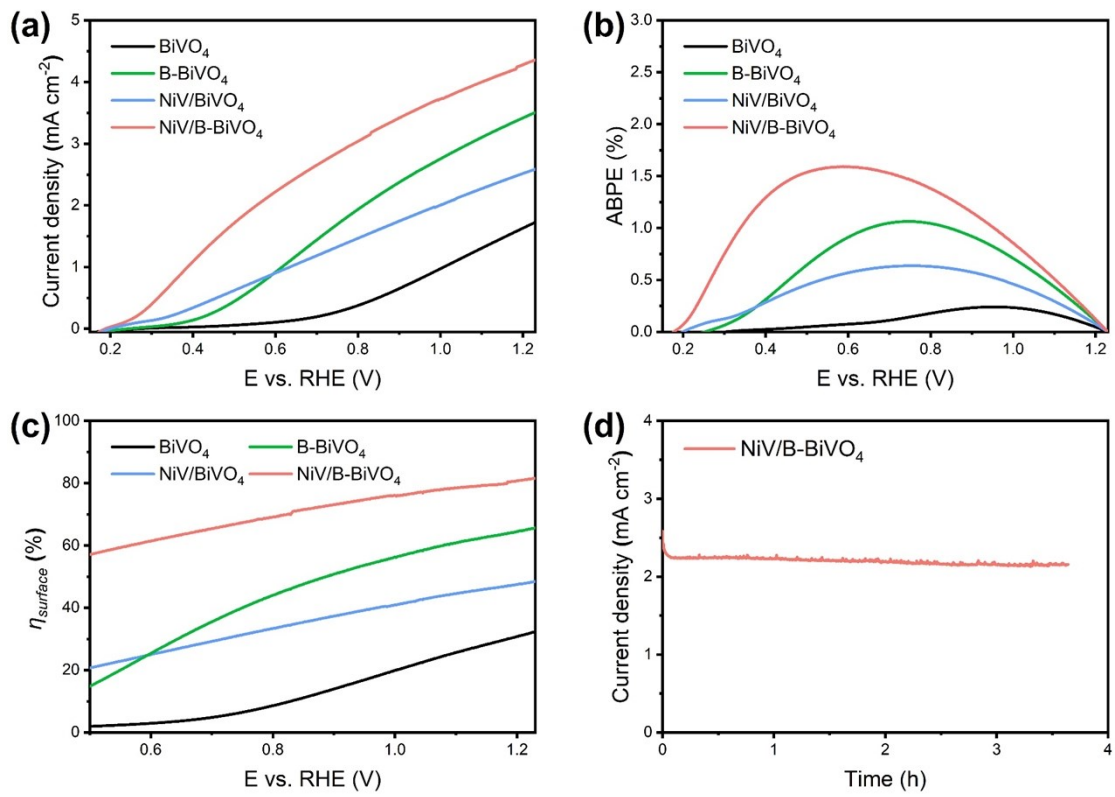


**Fig. S18.** **(a)** LSV curves of  $\text{BiVO}_4$ ,  $\text{B-BiVO}_4$ ,  $\text{NiV/BiVO}_4$ , and  $\text{NiV/B-BiVO}_4$  photoanodes under AM 1.5G illumination in a 1.0 M potassium borate buffer at pH 9.3 (scan rate:  $10 \text{ mV s}^{-1}$ ); **(b)** ABPE curves of photoanodes calculated from LSV curves; **(c)** Surface charge transfer efficiency ( $\eta_{\text{surface}}$ ) of photoanodes obtained from LSV curves of water oxidation and sulfite oxidation; **(d)** Long-term  $J-t$  curves at a constant bias of  $0.6 \text{ V}_{\text{RHE}}$ .

**Table S1.** PEC performance of LDH/BiVO<sub>4</sub> based photoanodes.

BiVO <sub>4</sub> photoanode	LDH co-catalyst loading method	$J_{ph}$ @1.23 V <sub>RHE</sub> (mA·cm <sup>-2</sup> )	Onset potential (V <sub>RHE</sub> )	Test condition <sup>[a]</sup>	Year
NiFeV/B-BiVO <sub>4</sub>	Drop casting (10 µg cm <sup>-2</sup> )	4.6	0.21	1.0 M KBi, pH 9.3	This work
CoAl/BiVO <sub>4</sub> <sup>1</sup>	Electrodeposition	3.5	0.41	0.5 M Na <sub>2</sub> SO <sub>4</sub> , pH 7.35	2021
NiFeY/BiVO <sub>4</sub> <sup>2</sup>	Hydrothermal	5.2	0.31	1.0 M KBi, pH 9.5	2020
Fe <sub>x</sub> Ni <sub>4-x</sub> -H/BiVO <sub>4</sub> <sup>3</sup>	Electrodeposition	3.65	0.53	0.5 M Na <sub>2</sub> SO <sub>4</sub> , pH 7	2020
ZnCoV/BiVO <sub>4</sub> <sup>4</sup>	Electrodeposition	2.55	0.33	0.1 M NaBi, pH 9.4	2020
NiFe/rGO/BiVO <sub>4</sub> <sup>5</sup>	Electrodeposition	3.26	0.4	1.0 M KBi, pH 9.33	2020
CoCe/BiVO <sub>4</sub> <sup>6</sup>	Hydrothermal	3.74	0.2	0.5 M KBi, pH 11	2020
NiCo/BiVO <sub>4</sub> <sup>7</sup>	Electrodeposition	2.95	0.4	0.5 M Na <sub>2</sub> SO <sub>4</sub> , pH 7.3	2020
CoMn/BiVO <sub>4</sub> <sup>8</sup>	Electrodeposition	2.69	0.31	0.5 M KPi, pH 7	2020
CoAl/GDY/BiVO <sub>4</sub> <sup>9</sup>	Hydrothermal	3.15	0.46	0.1 M Na <sub>2</sub> SO <sub>4</sub> , pH 6.8	2019
NiOOH/BP/BiVO <sub>4</sub> <sup>10</sup>	photodeposition	4.48	0.4	0.5 M KPi pH 7.1	2019
NiFe/BiVO <sub>4</sub> <sup>11</sup>	Drop casting	1.2	0.3	0.1 M KBi, pH 9.2	2018
CDs/NiFe/BiVO <sub>4</sub> <sup>12</sup>	Electrodeposition	2.84	0.5	0.5 M PBS, pH 7).	2018
CoPO <sub>3</sub> /pGO/NiFe/BiVO <sub>4</sub> <sup>13</sup>	Hydrothermal	4.45	0.17	1.0 M KBi, pH 9	2018
NiFe/BiVO <sub>4</sub> <sup>14</sup>	Hydrothermal	2.49	0.62	0.5 M Na <sub>2</sub> SO <sub>4</sub> , pH 7.3	2018
β-FeOOH/BiVO <sub>4</sub> <sup>15</sup>	Immersion	4.3	0.5	0.2 M Na <sub>2</sub> SO <sub>4</sub> , pH 7	2018
CoOOH/BiVO <sub>4</sub> <sup>16</sup>	Spin coating	4.0	0.2	0.2 M KPi, pH 7	2018
NiFe/BiVO <sub>4</sub> <sup>17</sup>	Hydrothermal	4.02	0.40	0.1 M KHCO <sub>3</sub> , pH 8.6	2017
CoLa/BiVO <sub>4</sub> <sup>18</sup>	Electrodeposition	2.02	0.19	0.5 M KPi, pH 7	2017

NiFe/BiVO <sub>4</sub> <sup>19</sup>	Electrodeposition	1.21	0.32	0.5 M Na <sub>2</sub> SO <sub>4</sub> , pH ~7	2017
CoFe/BiVO <sub>4</sub> <sup>20</sup>	Electrodeposition	2.48	0.23	0.5 M KPi, pH 7	2017
Ferrihydrite/BiVO <sub>4</sub> <sup>21</sup>	Hydrothermal	4.78	0.25	0.4 M NaBi pH 9	2017
QD/CoAl/BiVO <sub>4</sub> <sup>22</sup>	Hydrothermal	2.23	0.3	0.1 M KPi, pH 7	2016
CoAl/BiVO <sub>4</sub> <sup>23</sup>	Hydrothermal	1.1	0.41	0.1 M KPi, pH 7	2015
NiOOH/FeOOH/BiVO <sub>4</sub> <sup>24</sup>	Photodeposition	4.5	0.23	0.5 M KPi pH 7	2014

[a] NaBi= sodium borate; KPi= potassium phosphate; KBi= potassium borate; PBS=phosphate buffer solution.

\* Photocurrent density or onset potential was obtained from the J-V curves in the corresponding reference paper.

**Table S2.** Fitted results of the EIS curves in Fig. 3g

	BiVO <sub>4</sub>	B-BiVO <sub>4</sub>	NiFeV/BiVO <sub>4</sub>	NiFeV/B-BiVO <sub>4</sub>
R <sub>s</sub> / Ω	55.3	57.2	54.9	54.4
R <sub>ct</sub> / Ω	1398.2	518.1	372.6	289.2

## REFERENCES

1. P. Yue, H. She, L. Zhang, B. Niu, R. Lian, J. Huang, L. Wang and Q. Wang, *Appl. Catal. B: Environ.*, 2021, **286**, 119875.
2. D. He, R.-T. Gao, S. Liu, M. Sun, X. Liu, K. Hu, Y. Su and L. Wang, *ACS Catal.*, 2020, **10**, 10570-10576.
3. X. Ning, P. Du, Z. Han, J. Chen and X. Lu, *Angew. Chem. Int. Ed.*, 2021, **60**, 3504-3509.
4. T.-G. Vo, K.-F. Chang and C.-Y. Chiang, *J. Catal.*, 2020, **391**, 336-345.
5. H. Chen, S. Wang, J. Wu, X. Zhang, J. Zhang, M. Lyu, B. Luo, G. Qian and L. Wang, *J. Mater. Chem. A*, 2020, **8**, 13231-13240.
6. T. K. Sahu, S. Alam, D. Gogoi, N. R. Peela and M. Qureshi, *ACS Applied Energy Materials*, 2020.
7. H. She, P. Yue, X. Ma, J. Huang, L. Wang and Q. Wang, *Appl. Catal. B: Environ.*, 2020, **263**, 118280.
8. F. Zhao, N. Li, Y. Wu, X. Wen, Q. Zhao, G. Liu and J. Li, *Int. J. Hydrogen Energy*, 2020, **45**, 31902-31912.
9. J. Li, X. Gao, Z. Li, J. H. Wang, L. Zhu, C. Yin, Y. Wang, X. B. Li, Z. Liu and J. Zhang, *Adv. Funct. Mater.*, 2019, **29**, 1808079.
10. K. Zhang, B. Jin, C. Park, Y. Cho, X. Song, X. Shi, S. Zhang, W. Kim, H. Zeng and J. H. Park, *Nat. Commun.*, 2019, **10**, 2001.
11. T. S. Sinclair, H. B. Gray and A. M. Müller, *Eur. J. Inorg. Chem.*, 2018, **2018**, 1060-1067.
12. X. Lv, X. Xiao, M. Cao, Y. Bu, C. Wang, M. Wang and Y. Shen, *Appl. Surf. Sci.*, 2018, **439**, 1065-1071.
13. S. Ye, C. Ding, R. Chen, F. Fan, P. Fu, H. Yin, X. Wang, Z. Wang, P. Du and C. Li, *J. Am. Chem. Soc.*, 2018, **140**, 3250-3256.
14. Q. Wang, T. Niu, L. Wang, J. Huang and H. She, *Chinese J. Catal.*, 2018, **39**, 613-618.
15. Z. Beibei, W. Lei, Z. Yajun, D. Yong and B. Yingpu, *Angew. Chem. Int. Ed.*, 2018, **57**, 2248-2252.
16. F. Tang, W. Cheng, H. Su, X. Zhao and Q. Liu, *ACS Appl. Mater. Interfaces*, 2018, **10**, 6228-6234.
17. Y. Huang, Y. Yu, Y. Xin, N. Meng, Y. Yu and B. Zhang, *Sci. China Mater.*, 2017, **60**, 193-207.
18. M. Chhetri, S. Dey and C. N. R. Rao, *ACS Energy Lett.*, 2017, **2**, 1062-1069.
19. Y. Zhu, J. Ren, X. Yang, G. Chang, Y. Bu, G. Wei, W. Han and D. Yang, *J. Mater. Chem. A*, 2017, **5**, 9952-9959.
20. W. Liu, H. Liu, L. Dang, H. Zhang, X. Wu, B. Yang, Z. Li, X. Zhang, L. Lei and S. Jin, *Adv. Funct. Mater.*, 2017, **27**, 1603904.
21. F. Yu, F. Li, T. Yao, J. Du, Y. Liang, Y. Wang, H. Han and L. Sun, *ACS Catal.*, 2017, **7**, 1868-1874.
22. Y. Tang, R. Wang, Y. Yang, D. Yan and X. Xiang, *ACS Appl. Mater. Interfaces*, 2016, **8**, 19446-19455.
23. W. He, R. Wang, L. Zhang, J. Zhu, X. Xiang and F. Li, *J. Mater. Chem. A*, 2015, **3**, 17977-17982.
24. T. W. Kim and K.-S. Choi, *Science*, 2014, **343**, 990-994.